Pergamon

0956-7151(95)00157-3

Acta mater. Vol. 44, No. 1, pp. 43–56, 1996
Elsevier Science Ltd

1359-6454/96 $15.00 + 0.00

MICROCRACKING DUE TO GRAIN BOUNDARY SLIDING IN POLYCRYSTALLINE ICE UNDER UNIAXIAL COMPRESSION

A. A. ELVIN[1] and S. SHYAM SUNDER[2]

[1]Massachusetts Institute of Technology, Department of Civil and Environmental Engineering, Room 5-330A, Cambridge, MA 02139 and [2]NIST, Room B350, Building 226, Gaithersburg, MD 20899, U.S.A.

(Received 31 October 1994; in revised form 28 March 1995)

Abstract—This paper examines grain boundary sliding as a mechanism for nucleation and growth of microcracks in polycrystalline S2 ice, under uniaxial compression. The loading rate is fast enough so that the polycrystal response is almost linear. A unit cell model is set up and the resulting boundary value problem solved using the finite element method. Simulations show that by allowing grain boundary sliding a defect originating at the triple point grows stably, reaches a critical length and then propagates unstably to the neighboring triple point. The influence of the elastic mismatch between neighboring grains on microcracking stress is not strong. The stress causing microcrack growth is found to be inversely proportional to the square root of the grain size. If no grain sliding takes place, and only the elastic anisotropy mechanism operates, the stresses required for microcrack nucleation and growth are unrealisticly high; the resulting microcracks are also too short.

1. INTRODUCTION

The deformation of polycrystalline ice is highly non-linear and depends on the loading rate and temperature, as well as on the granular microstructure. While at low loading rates (less than $\sim 10^{-3}\,s^{-1}$ in compression) ice is ductile, it fails brittlely at higher rates and lower temperatures. The maximum stresses occur in the ductile-to-brittle transition regime. Under compression, microcrack accumulation is observed in this regime. Experimental evidence in [1] suggests two independent families of microcracks which nucleate in polycrystalline ice. The first microcrack family is independent of creep strain, while the second is dependent on it.

The nucleation of microcracks, which are dependent on creep strain, has been attributed to the dislocation pile up mechanism [2, 3] and to grain boundary sliding [4, 5]. Both these mechanisms were postulated for low strain rate loading where the polycrystal behaves in a ductile manner.

The elastic anisotropy mechanism has been postulated in Refs [3, 6] to be responsible for the formation of the strain-independent microcracks. This mechanism was thought to be dominant during high strain rate loading. More recently however, the stress fields which arise in the grains due to the actual anisotropy found in ice was analyzed in [7]. In this reference it was concluded that the mismatch in elastic moduli between neighboring grains in ice, under plane strain conditions, is not high enough to form precursor cracks.

This paper conducts a theoretical investigation of microcrack nucleation and growth in fresh water polycrystalline S2 ice at the high end of the ductile-to-brittle transition where the response is almost linear. Since the elastic anisotropy mechanism acting alone is not strong enough to nucleate precursor cracks, grain boundary sliding is investigated as a possible cause of microcracking. Only uniaxial compressive loading is considered. The aim is to predict at what stress microcracks nucleate and grow. The role of grain anisotropy and the effect of grain size on this stress is studied.

Polycrystalline ice, even that prepared in the laboratory, is a porous material. The bubble size and density is a function of freezing rate and the bubble shape can be approximated by cylinders or prolate spheroids [8]. Reference [9] studies isotropic polycrystalline ice with equiaxed grains prepared in the laboratory, and reports average bubble diameters of 0.06 and 0.12 mm for grain sizes between 1 and 2 mm and 2 and 7.3 mm, respectively. The bubble density is 2000 and 350 bubbles/cm^3 respectively. The nucleation and growth of a microcrack from a circular hole in an isotropic material is modeled in [10]. The minimum nucleation stress predicted by [10] under uniaxial compression using homogenized properties of ice is an order of magnitude larger than observed experimentally. At this stress level the microcrack length is of the order of 0.18 bubble diameters, viz. 0.018 mm, as compared with experimentally observed microcracks which are of the order of the grain size [11], viz. of the order of millimeters. The effect of including the local inhomogeneity of the ice grains, as

well as grain boundary sliding, on a microcrack originating from a bubble, is studied in this paper.

The stresses arising in a polycrystal array are studied using a repetitive unit cell model. The concept of the unit cell is well known; the work reported in [12] on ceramics and in [7] on saline ice is closest to this study. The major difference between this work and these references is the modeling of grain boundary sliding. Of course differences in the size and physical details of the unit cell also exist; the present paper models anisotropic grains and air bubbles located at the triple points.

The organization of this paper is as follows. The unit cell model is developed in Section 2: the physical details of the unit cell are described and the motivation for the grain boundary sliding mechanism is given. Section 3 formulates the unit cell as a boundary value problem, describes the method of analysis of the boundary value problem, and states the criterion for microcrack nucleation and growth. The discussion of the results is presented in Section 4 after first describing the material parameters. The effects of preventing grain boundary sliding and the question of simultaneous coexistence of grain boundary sliding and elastic behavior of the polycrystal is addressed in Section 4.2. The effects of grain anisotropy and grain size on the stresses required for microcrack nucleation and growth are discussed in Sections 4.2 and 4.3 respectively.

2. THE UNIT CELL MODEL

The whole domain is subdivided into repetitive unit cells (see Fig. 1). The response of the entire domain to far field loading can be obtained by analyzing only the unit cell. In order to define the unit cell, an assumption has to be made on the size of the repetitive cell. This size fixes the number of grains and hence the number of grain orientations modeled.

2.1. Physical details of unit cell

In this paper the grain geometry is idealized by hexagons. The unit cell is made up of three grains with orientations ζ_A, ζ_B, and ζ_C; see Fig. 1 and for details Fig. 2(a). The assumption of modeling only three grain orientations is not as restrictive as it first appears, since: (i) the individual ice crystals exhibit weak elastic anisotropy, and (ii) the effect of anisotropy on microcracking is not strong (see details in Section 4.3).

The unit cell is assumed to be under plane stress conditions. This is consistent with the microstructure of transversely isotropic S2 ice where the cell lies in the plane of polycrystal isotropy.

Observations show that bubbles have a tendency to concentrate on grain boundaries, especially at geometric discontinuities. In the unit cell, cylindrical air bubbles are located at triple points in the interior of the cell (at TP1 and TP2 in Fig. 3). These bubbles extend through the thickness of the cell.

The ice surface contains flaws in the form of steps, pits and ledges. The steps can have a depth ranging from 0.1 to 4 μm [13]. Such flaws are likely to be present on the bubble surface and might nucleate into microcracks. The details of the triple point TP1 containing a bubble with a microcrack are shown in Fig. 2(b). At the start of microcracking, the microcracks are far apart. Thus only a single microcrack emanating from TP1 is considered in this paper.

2.2. Grain boundary sliding

Grain boundaries are zones of finite volume where the material is highly disordered when compared with the material inside the grains. The grain boundary thickness has been predicted [14] to be of the order of a fraction to a few microns in thickness and to be dependent on temperature and salinity. Due to the disorder, the entropy of the grain boundaries is higher than that of the grain. Hence the elastic stiffness moduli of the grain boundary zone are expected to be lower than those of the grain.

Naturally occurring polycrystalline ice is typically found in the temperature range $0°C \geqslant T \geqslant -40°C$. This corresponds to a homologous temperature range of $1 \geqslant T_h \geqslant 0.85$. The behavior of the grain boundary zone in polycrystalline ice is very complex and its nature is not fully understood. The grain boundary zone is sensitive to temperature. There is

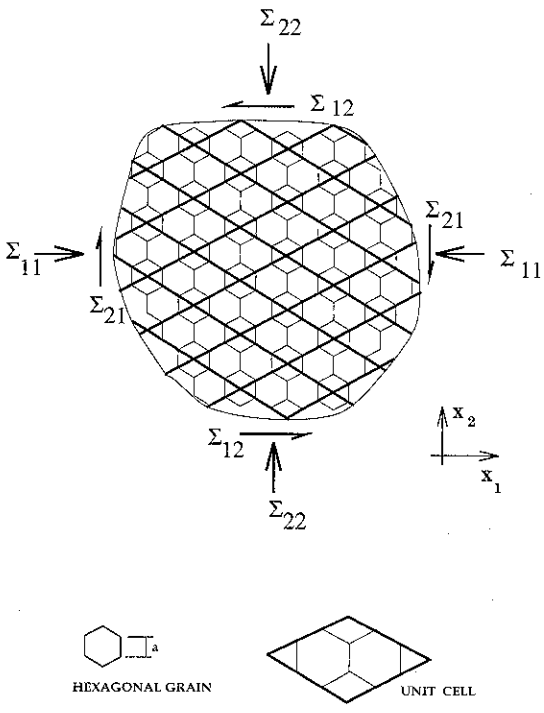

Fig. 1. The polycrystalline domain of hexagonal grains showing the mosaic of repetitive unit cells.

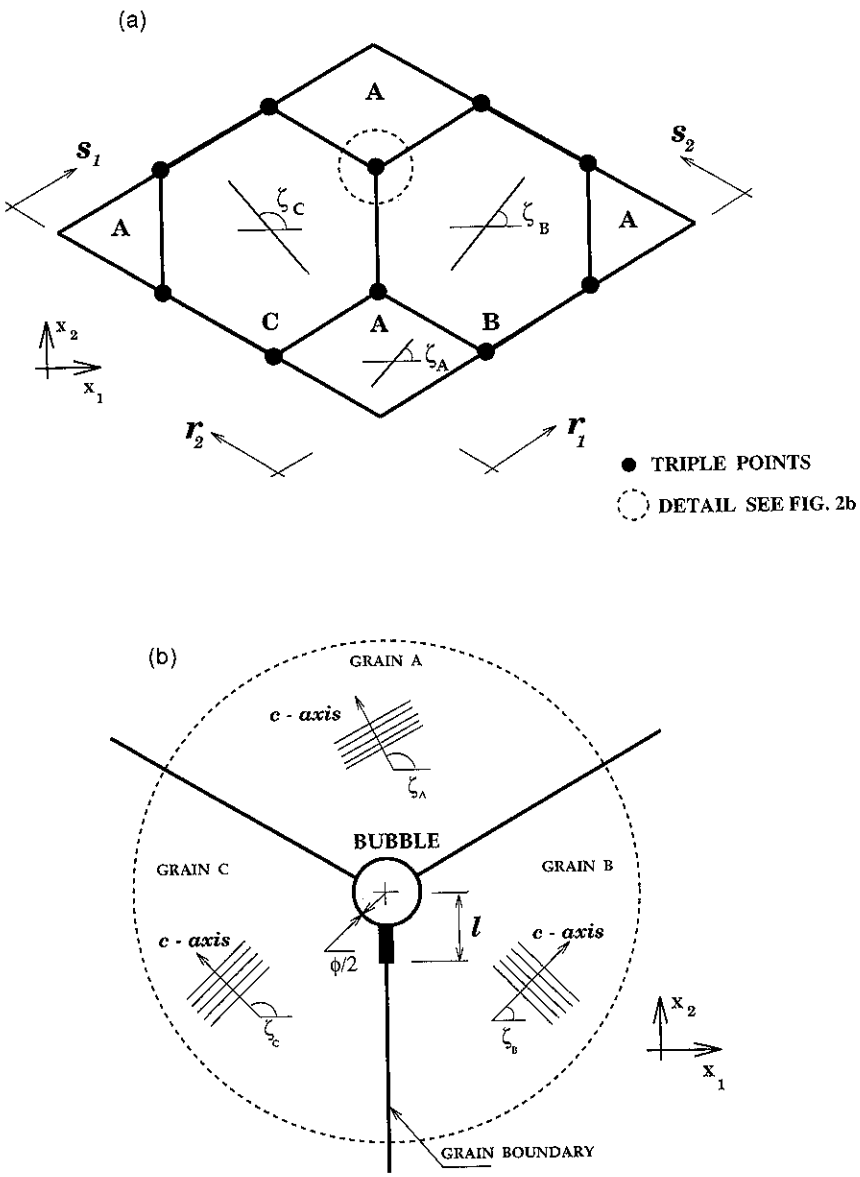

Fig. 2. (a) The unit cell model. (b) Detail of a triple point junction located within the unit cell.

experimental evidence of a liquid, or a quasi-liquid, layer on the grain boundaries at temperatures above -10°C (see the references in the review article [15]). Such a layer would promote grain boundary sliding.

From internal friction experiments on single and polycrystalline ice, a relaxation phenomenon associated only with grain boundaries was deduced in [16]. By measuring the Young's modulus, Gold and Traetteberg [17] found two active relaxation processes both in columnar grained and in isotropic equiaxed polycrystalline ice. The first process has a relaxation time of the order of 1 s, while the second is associated with a much longer time period. These authors observed that the time dependence of Young's modulus for times greater than 0.1 s is dominated by the second, i.e. slower, relaxation process.

The duration of high strain rate tests, where the response of the polycrystal is almost linear and the sample fails in a brittle manner, is typically less than a few seconds. Brittle behavior is observed when the applied strain rates are in the range $10^{-3}\,s^{-1} \leqslant \dot{\epsilon} \leqslant 10^{-1}\,s^{-1}$ (see for example the work of Schulson and co-workers). For these short durations, the first relaxation phenomenon observed in [16] must be active; this relaxation process might be associated with grain boundary sliding. During the progress of this work it has come to the authors' attention that visco-elastic grain boundary sliding has been observed at $\dot{\epsilon} = 10^{-2}\,s^{-1}$ and $\dot{\epsilon} = 10^{-3}\,s^{-1}$ at $T = -10$°C

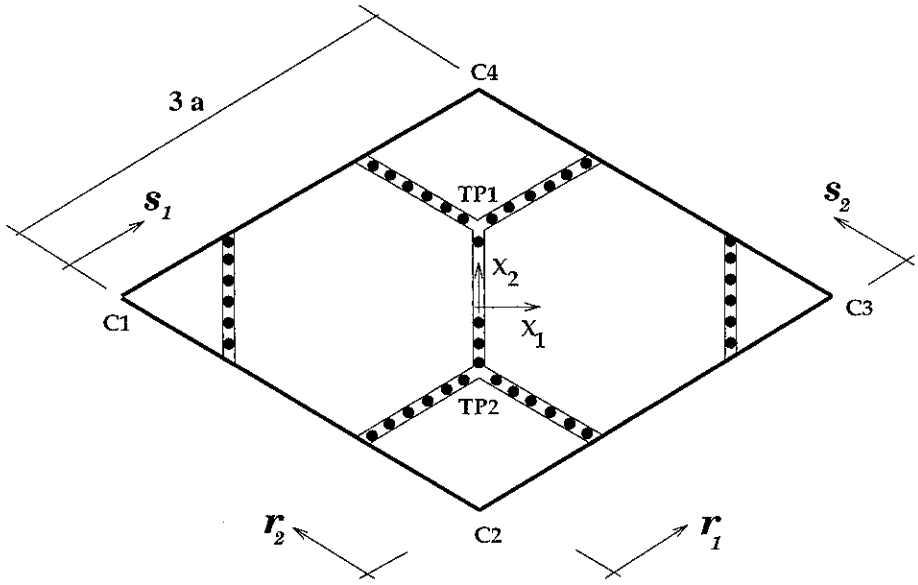

Fig. 3. A schematic representation of the unit cell with rollers on the grain boundaries.

by Picu and Gupta [18]†. The seemingly contradictory simultaneous occurrence of grain boundary sliding and linear response of the polycrystal will be explored in Section 4.2 after the unit cell model has been fully described.

In the unit cell the grain boundary region can be modeled as a linear visco-elastic material. However, since the material parameters of the grain boundary are not known, and for simplicity, the grain boundaries are assumed to be fully relaxed. Thus in the model the grain boundaries cannot transfer shear stresses. This assumption should underpredict the stresses that cause microcrack nucleation and growth. Further, since the grain boundary thickness (order of micrometers) is much smaller than the dimensions of the grain (order of millimeters), and since the shear resistance of the grain boundary is assumed to be negligible, the grain boundary thickness is ignored in the unit cell model.

3. MICROCRACK NUCLEATION AND GROWTH

In order to determine the microcrack nucleation stress, the stresses required to extend the microcrack and the path of the microcrack, the spatial distributions of stress, strain and displacement, within the unit cell, are required. The geometry of the unit cell has already been defined. In this section the unit cell boundary value problem is first formulated and then solved using the finite element method. The criterion for crack nucleation and growth is then presented.

†These authors attribute stable microcrack nucleation to grain boundary sliding.

3.1. Formulation and analysis of the unit cell boundary value problem

The polycrystalline aggregate (see Fig. 1) is subjected to uniaxial far field stress, Σ_{22} with no confinement $\Sigma_{11} = 0$ and no shear $\Sigma_{12} = 0$. Advantage can be taken of the repetitive nature within the aggregate; only a single unit cell needs to be considered.

Equilibrium within the cell is automatically met by satisfying the principle of virtual work

$$\int_A \delta\epsilon \cdot \sigma \, dA = \int_S \delta\mathbf{u} \cdot \mathbf{T} \, dS \tag{1}$$

where $\delta\epsilon$ and σ are the virtual strain and stress tensors at a point, $\delta\mathbf{u}$ is the virtual displacement and $\mathbf{T}$ is the surface traction. Integration is performed over the entire unit cell area, A, and over the entire boundary length S. The elastic stress–strain relation for a grain is

$$\sigma = \mathbf{C}_g(\zeta)\epsilon \tag{2}$$

where $\mathbf{C}_g(\zeta)$ is the elastic stiffness tensor of a single grain in the global reference frame and it depends on the basal plane orientation, ζ [see Fig. 2(b)]. Substituting equation (2) into equation (1), the principle of virtual work to be satisfied, is

$$\int_A \delta\epsilon \cdot [\mathbf{C}_g(\zeta)\epsilon] \, dA = \int_S \delta\mathbf{u} \cdot \mathbf{T} \, dS. \tag{3}$$

Traction boundary conditions corresponding to far field loading are applied to the sides of the unit cell. Reference labels of points are shown in Fig. 3.

Along sides C1–C4 and C4–C3

$$T_1 = 0, \quad T_2 = -\Sigma_{22}. \tag{4}$$

Along sides C1–C2 and C2–C3

$$T_1 = 0, \quad T_2 = \Sigma_{22}. \tag{5}$$

In addition the following displacements are prescribed:

Point C1, the center of grain A, is pinned

$$u_1 = u_2 = 0. \tag{6}$$

Displacement of Point C3

$$u_2 = 0. \tag{7}$$

Free grain boundary sliding is allowed by specifying rollers on the grain boundaries (see Fig. 3). These rollers cannot transfer shear tractions but can transfer both tensile and compressive normal tractions. Note that Fig. 3 is schematic; the grain boundary thickness is assumed to be zero. The free sliding conditions on the grain boundaries located on the perimeter of the cell are specified below.

The boundaries of the unit cell have to be constrained to maintain compatibility with neighboring cells. To this end, length measures along the perimeter of the cell are defined (see Fig. 3): r_1 and r_2 from Point C2, and s_1 and s_2 from Points C1 and C3, respectively. Compatibility is maintained within grain A if:

In the ranges $0 \leqslant r_1 \leqslant a$ and $2a \leqslant r_1 \leqslant 3a$

$$u_1(r_1) - u_1(\mathrm{C2}) = u_1(s_1) - u_1(\mathrm{C1})$$
$$u_2(r_1) - u_2(\mathrm{C2}) = u_2(s_1) - u_2(\mathrm{C1}). \tag{8}$$

In the ranges $0 \leqslant r_2 \leqslant a$ and $2a \leqslant r_2 \leqslant 3a$

$$u_1(r_2) - u_1(\mathrm{C2}) = u_1(s_2) - u_1(\mathrm{C3})$$
$$u_2(r_2) - u_2(\mathrm{C2}) = u_2(s_2) - u_2(\mathrm{C3}). \tag{9}$$

To allow slip on grain boundaries found on the perimeter of the cell, and to maintain compatibility with neighbors, the following constraints on deformations are required:

In the range $a \leqslant r_1 \leqslant 2a$

$$u_2(r_1) - u_2(\mathrm{C2}) - u_2(s_1) + u_2(\mathrm{C1})$$
$$= \frac{1}{\sqrt{3}}[u_1(r_1) - u_1(\mathrm{C2}) - u_1(s_1) + u_1(\mathrm{C1})]. \tag{10}$$

In the range $a \leqslant r_2 \leqslant 2a$

$$u_2(r_2) - u_2(\mathrm{C2}) - u_2(s_2) + u_2(\mathrm{C3})$$
$$= \frac{1}{\sqrt{3}}[u_1(r_2) - u_1(\mathrm{C2}) - u_1(s_2) + u_1(\mathrm{C3})]. \tag{11}$$

The average axial strain, $\bar{\epsilon}_{22}$, experienced by the unit cell is defined as

$$\bar{\epsilon}_{22} = \frac{1}{6a}\int_0^{3a} \frac{u_2(3a - s_2) - u_2(r_1)}{3a - r_1}\,\mathrm{d}r_1 + \frac{1}{6a}\int_0^{3a} \frac{u_2(3a - s_1) - u_2(r_2)}{3a - r_2}\,\mathrm{d}r_2 \tag{12}$$

where $(\cdot)$ is the argument of the function u_2. The displacement component, u_2 is defined on the cell perimeter and the length measures r and s can be interchanged. The integration is performed numerically and Points C1 and C3 are excluded.

The finite element method is used to solve the boundary value problem defined by equation (3) subjected to boundary conditions given in equations (4)–(11). A typical mesh containing 388 elements is shown in Fig. 4(a). Figure 4(b) shows the refined mesh around the bubble containing the microcrack. The discretization is conducted so that the elements do not intersect the grain boundaries. The mesh contains standard eight node isoparametric elements. At the crack tip eight, singular, quarter-point elements are used. Full 3×3 Gauss integration is performed. The discretization ensures that a node found at a distance r_1 from C2 will have a counterpart at the same distance s_1 from C1; the same applies to r_2 and s_2.

The level of discretization, and the imposition of the boundary conditions on the unit cell have been checked as follows. First, the finite element solution with no grain boundary sliding and isotropic homogeneous grains compares well with the known analytical solution of the stress distribution around a circular hole. In the numerical solution, although the domain contains multiple holes, their diameter is small compared to the distance between them and hence their effect on each other is negligible. Second, when grain boundary sliding is allowed, the compatibility of deformations on the boundary

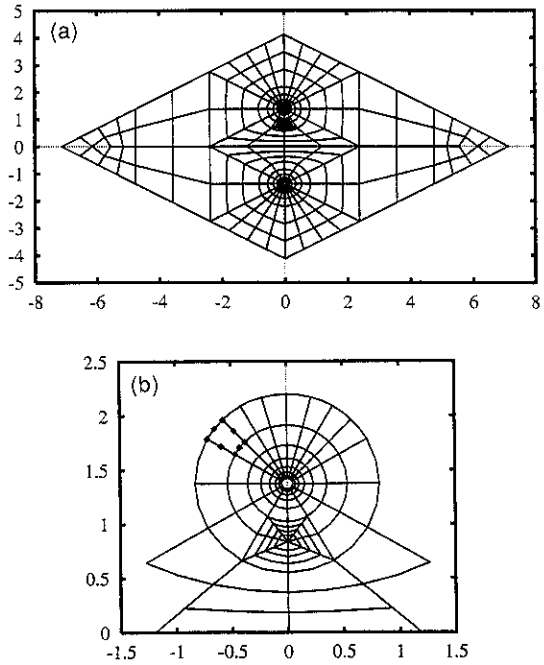

Fig. 4. (a) Finite element discretization of the unit cell. (b) Detail of finite element discretization around the bubble and the microcrack.

of neighboring unit cells has been checked. Finally, for a symmetric distribution of grain orientations about the line C2–C4, and for a symmetric far field loading, the symmetry of the solution has been verified.

3.2. Criterion for microcracking

The nucleation of the flaw located at the triple point and the propagation of the resulting microcrack occurs when the energy released in forming the crack is greater than the surface energy of the material. Even though the far field stress is uniform, locally the stress state is not homogeneous. This is due to grain anisotropy and discontinuities such as grain boundaries. Further the material resistance to cracking is not homogeneous; the fracture surface energy of the grain boundary is less than that of the grain. Thus, in general, the flaw and the microcrack are under mixed Mode I and Mode II loading, and microcrack extension is not necessarily collinear with the original crack.

Path independent integrals can provide a measure of the amount of energy released in extending a crack. Such an energy release criterion can be stated as [19, 20]: the crack will grow in the direction in which the components of the energy release vector equals the fracture surface energy. It has been shown in [21] that the energy release rate per unit crack tip extension in two mutually perpendicular directions, x and y is given by

$$J_x = \oint_\Gamma U\,\mathrm{d}y - \boldsymbol{\sigma}\mathbf{n}\cdot\frac{\partial \mathbf{u}}{\partial x}\,\mathrm{d}\Gamma$$

$$J_y = -\oint_\Gamma U\,\mathrm{d}x + \boldsymbol{\sigma}\mathbf{n}\cdot\frac{\partial \mathbf{u}}{\partial y}\,\mathrm{d}\Gamma \qquad (13)$$

where U is the strain energy density, $\mathbf{n}$ is the outward unit normal to the counter clockwise integration path, Γ, and $\mathrm{d}\Gamma$ is the arc length along Γ. Note that J_x is the conventional J integral [22].

The components of the **J** vector can be combined to give the energy released in a direction β (from Fig. 24.3 in [20], and [19]

$$\mathcal{G}(\beta) = J_x\cos(\beta) + J_y\sin(\beta) \qquad (14)$$

where β is measured from the x-axis. The crack will extend in a direction β when

$$2\gamma(\beta) = \mathcal{G}(\beta) \qquad (15)$$

where $\gamma(\beta)$ is the fracture surface energy; it depends on whether the crack is extending along the grain boundary or into the grain.

The components of the path independent **J** vector, equation (13), are calculated numerically from the finite element analysis. Three different paths are considered in computing the **J** components. All paths are taken through the Gauss points and pass through the centers of the elements. In this paper, the variation of **J** in most cases is less than 1%; in the worst case the variation is 4.5%.

In the simulations of microcracking, a constant compressive uniaxial far field stress, Σ_{22}, is applied to the polycrystal. The microcrack is extended, and the corresponding **J** vector computed. The result is $\mathcal{G}(\beta)$ as a function of crack length, l. The stress required for microcrack nucleation and propagation, Σ^*, is obtained by scaling the applied far field stress as follows

$$\Sigma^* = \Sigma_{22}\sqrt{\frac{2\gamma(\beta)}{\mathcal{G}(\beta)}}. \qquad (16)$$

The above analysis predicts the stress, Σ^*, required to realize a microcrack of length, l, as well as providing information on the stability and trajectory of the microcrack.

4. SIMULATION OF NUCLEATION AND GROWTH OF A MICROCRACK

The effects of grain boundary sliding, grain anisotropy, and grain size on microcrack nucleation and growth are studied in this section. The applied loading rate is assumed to be sufficiently high so as to correspond to the brittle end of the ductile-to-brittle regime. Compressive stresses and strains have positive values in this section.

4.1. Material parameters

The material parameters used in all numerical simulations are identified here. Two groups of material parameters are required: (i) the elastic stiffness; and (ii) fracture surface energies.

The dynamic elastic stiffness of a single ice crystal was measured using Brillouin spectroscopy [23]. At -16°C Ref. [23] reports the single crystal stiffness to be

$$\mathbf{C}_g(\zeta = 0°) = \begin{bmatrix} 15.010 & 5.765 & 5.765 & & & \\ & 13.929 & 7.082 & & 0 & \\ & & 13.929 & & & \\ & & & 3.4235 & & \\ & \text{sym.} & & & 3.014 & \\ & & & & & 3.014 \end{bmatrix} \text{GPa} \qquad (17)$$

where $x_2 - x_3$ is the isotropy plane in the transversely isotropic crystal; the c-axis lies in the x_1 direction ($\zeta = 0°$). The above elastic constants are mildly temperature dependent. The following empirical relationship for the stiffness at temperature T is obtained [23]

$$\mathbf{C}_g(T) = \mathbf{C}_g(T_{ref}) \frac{(1 - 1.418 \times 10^{-3} T)}{(1 - 1.418 \times 10^{-3} T_{ref})} \quad (18)$$

where T_{ref} is the temperature at which $\mathbf{C}_g$ is known ($T_{ref} = -16°C$), and all temperatures are measured in °C. Equation (18) shows that between 0 and −20°C the variation in dynamic stiffness of a single crystal is practically negligible.

Reducing the single crystal stiffness to plane stress conditions ($\sigma_{33} = 0$) with $x_1 - x_2$ being the plane of interest, the following dynamic single crystal plane stress stiffness is obtained

$$\mathbf{C}_g(\zeta = 0°) = \begin{pmatrix} 12.624 & 2.832 & 0 \\ 2.832 & 10.328 & 0 \\ 0 & 0 & 3.014 \end{pmatrix} \text{GPa}. \quad (19)$$

The surface energies for ice at temperatures close to 0°C were determined from experimental measurements in [24]. The following surface energies are reported:

$$\text{Grain boundary } \gamma_{gb} = 0.065 \text{ J/m}^2$$

$$\text{Solid vapor, or crystal } \gamma_{sv} = 0.107 \text{ J/m}^2.$$

Experiments reported in [25] on single crystals of ice at −196°C show that microcracks do not have any preferred orientation and do not follow any particular crystallographic plane. From this observation, the variation of the surface energy with orientation within the crystal will be ignored in the simulations. Further, the surface energies reported in [24] might be temperature sensitive; currently no data is available on this sensitivity. Since surface energy is proportional to stiffness, and the variation in stiffness in the range 0°C to −20°C is negligible [equation (18)], the surface energies in this range are assumed to be constant. This is a strong assumption since the properties of the grain boundaries are expected to be effected by temperature.

4.2. *Effect of grain boundary sliding*

The assumption of relaxed grain boundaries allows free slip to occur between grains. Thus no shear stress can be transferred from grain to grain and this effects the Young's modulus of the polycrystal. Reference [26] idealized the isotropic grains by spheres, and obtained an analytical solution for the relaxed Young's modulus. The results in [26] show that the ratio of relaxed to unrelaxed Young's modulus, E_R/E, is a function of Poisson ratio only; for a Poisson ratio of 0.33, $E_R/E = 0.64$. The effect on Young's modulus, of fully relaxed grain boundaries, in a *hexagonal* array of grains can be determined using the unit cell model.

The Young's modulus of the polycrystal is calculated from the average quantities:

$$E = \frac{\Sigma_{22}}{\bar{\epsilon}_{22}} \quad (20)$$

where the average strain, $\bar{\epsilon}_{22}$, is given by equation (12). The relaxed Young's modulus is determined by leaving the constraint boundaries of the unit cell unchanged. To determine the unrelaxed Young's modulus all the rollers on the grain boundaries within the unit cell are removed. Also, on the perimeter of the unit cell the sliding constraint conditions given by equations (10) and (11) are replaced by no sliding constraints equations (8) and (9).

Simulations show that $E_R/E = 0.93$ for isotropic hexagonal grains with a Poisson ratio of 0.33. Analyzing an anisotropic, non-homogeneous polycrystal with $\zeta_B = -\zeta_C$ and $\zeta_A = 0$, also shows that the difference between relaxed and unrelaxed modulus is less than 10%. The amount of relaxation is less than in [26] because in a hexagonal array, with assumed zero grain boundary thickness, there is no relative motion between the grains at each triple point. In reality the grain boundary layer has a finite volume which is much smaller than the volume of the crystal. Hence a compliant grain boundary zone will have only a small effect on the volumetric average of the overall elastic moduli. Further, the unit cell model with fully relaxed grain boundaries, prior to microcrack nucleation, shows *linear* behavior. These results of a small reduction in Young's modulus and linear behavior (i.e. creep strains insignificant) are consistent with experimental observations of ice loaded at high strain rates.

The possibility of a microcrack nucleating from a bubble located at a triple point surrounded by randomly oriented anisotropic grains with *no grain boundary sliding* has been studied. As already mentioned, the work in [10] on a circular hole in an isotropic homogeneous material predicts the *minimum* nucleation stress to be 11.8 MPa†. The *maximum possible* microcrack length is approximately three bubble diameters, which is an order of magnitude shorter than typical lengths observed in ice. By including the bubble and random grain orientations in the unit cell, a much larger local tensile field develops around the microcrack under far field uniaxial compression. In general the microcrack is under mixed mode loading. The stresses required to propagate the microcrack so determined, are lower than those predicted using the expression in [10], but they are still approximately an order of magnitude higher (depending on the orientations of the grains) than experimental observations. The maximum possible

†The isotropic microfracture toughness for ice is taken as $K_{ic} = 40 \text{ kPa}\sqrt{\text{m}}$ based on the surface energy reported in [24] and a homogenized Young's modulus of $E = 9.5$ GPa; the bubble diameter, $\phi = 0.1$ mm consistent with observations in [9].

length of the microcrack is also longer than in the isotropic homogeneous case, but is still much shorter than the grain facet.

The above discussion is reinforced by considering the distribution of the stress component σ_{11} in the vicinity of the triple point. The stress component σ_{11} is considered because it provides Mode I loading on a grain boundary crack. This stress component is normalized by the far field loading, Σ_{22}. A grain size of $d = 5$ mm is considered with a symmetric distribution of grain orientations: $\zeta_B = -\zeta_C = 150°$ and $\zeta_A = 0°$. Contour plots of the normalized σ_{11}/Σ_{22} are shown in Fig. 5. The variations of σ_{11}/Σ_{22} along the line $x = 0$ are also shown.

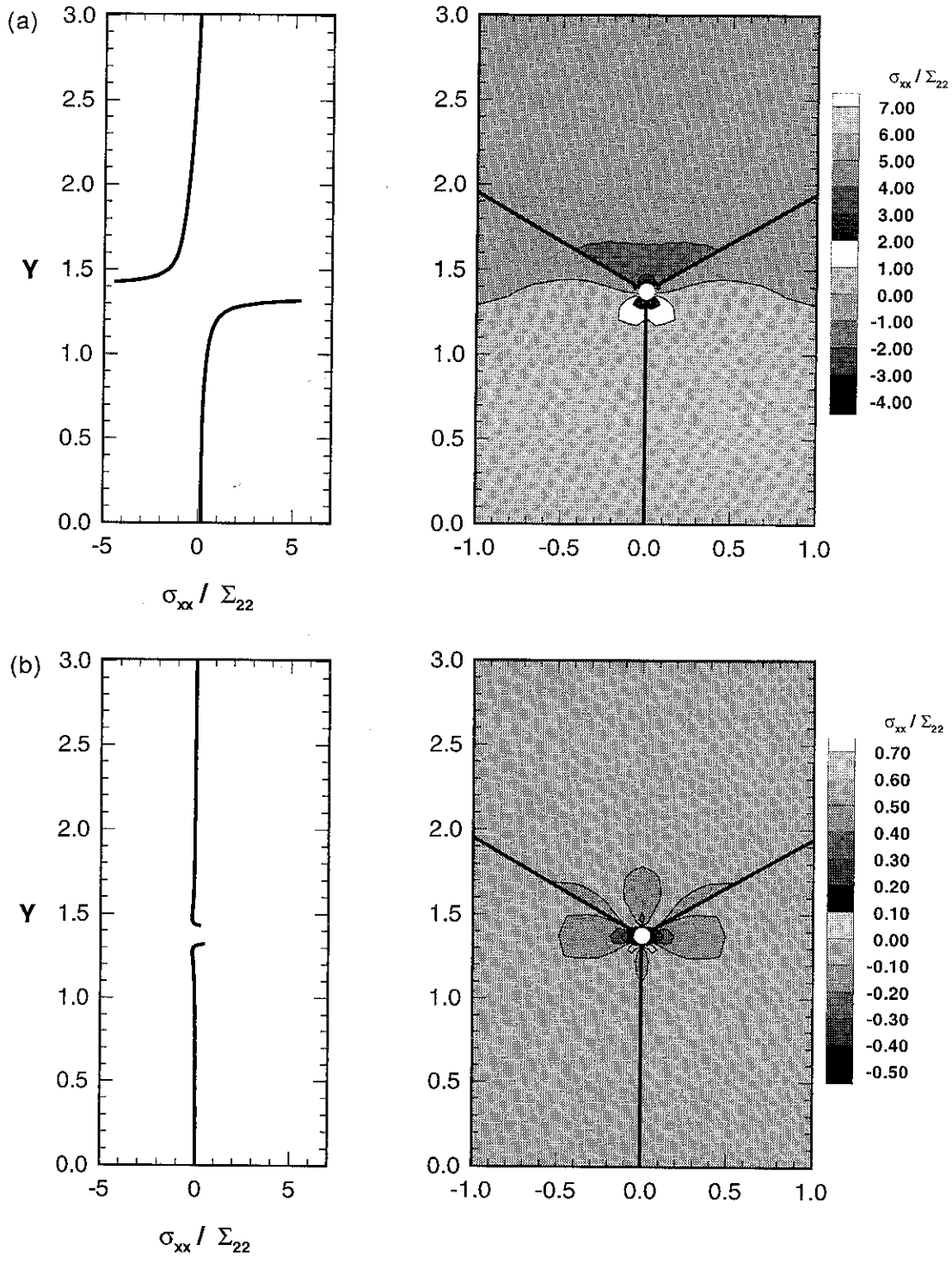

Fig. 5a and b

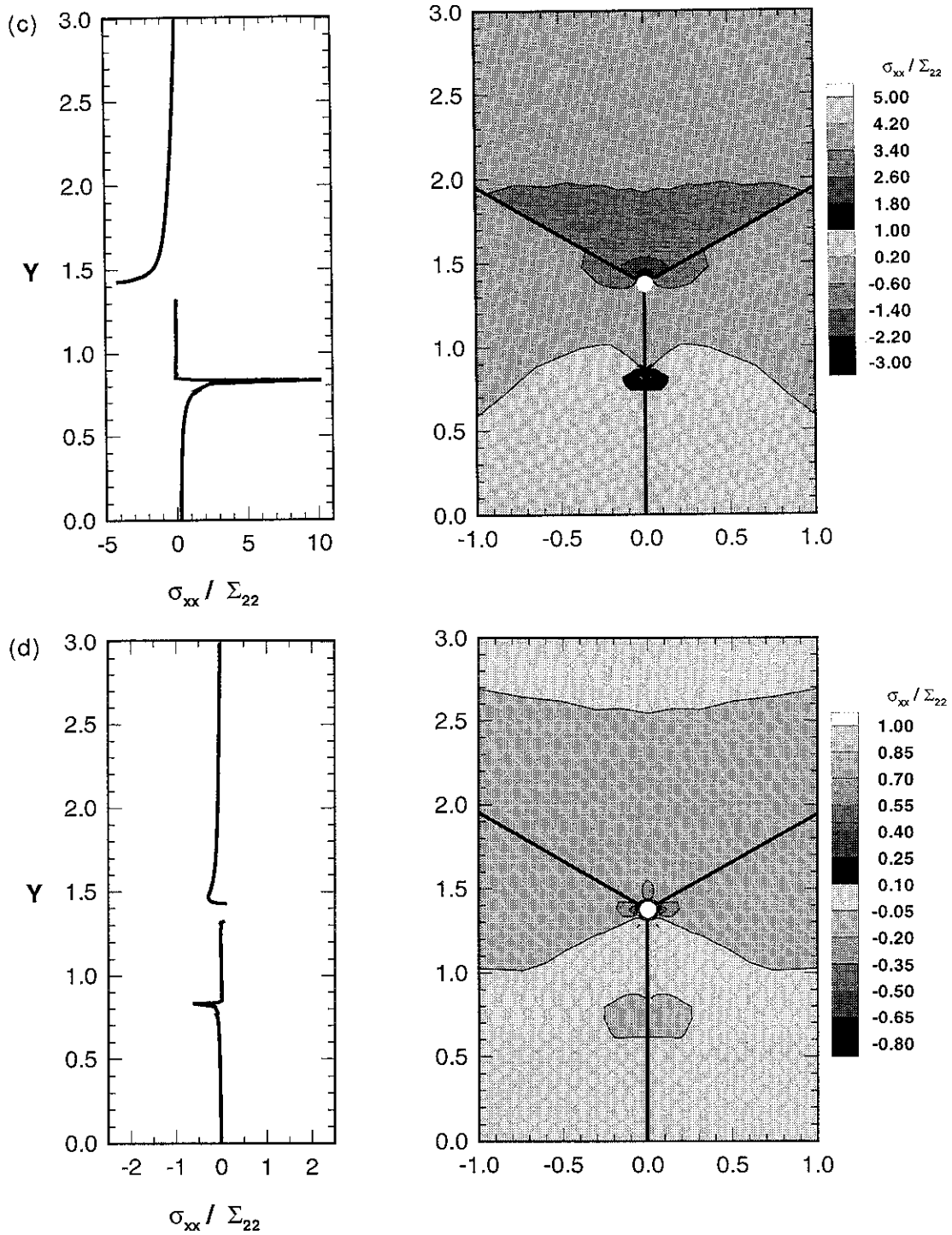

Fig. 5. Variation of σ_{11}/Σ_{22} in the vicinity of a triple point, $d = 5$ mm, $\zeta = 150°$: (a) grain boundary sliding permitted and no microcrack present; (b) no grain boundary sliding permitted and no microcrack present; (c) grain boundary sliding permitted and a microcrack is present; (d) no grain boundary sliding permitted and a microcrack is present.

In Fig. 5(a, c) grain boundary sliding is permitted. In Fig. 5(b, d) no grain boundary sliding is permitted. In Fig. 5(c, d) a microcrack emanates from the hole; the microcrack length normalized by the facet length is $l/a = 0.196$.

Figure 5 shows that by allowing grain boundary sliding, the stress is concentrated by the hole to a much greater extent than when no sliding is allowed. The grain boundary sliding mechanism causes a wedging action; at a triple point, one grain is in

compression, while the other two are wedged apart and hence are in tension. This tension persists over the entire grain boundary when sliding is allowed. On the other hand, with no grain boundary sliding, σ_{11} soon falls to zero.

It is important to note that the effect of the hole is local. If a microcrack is present when grain boundary sliding is allowed [Fig. 5(c)], the tensile stress along the grain boundary ensures that the crack is *open*. Hence the singularity at the crack tip is positive. In the no sliding case, a small but compressive local σ_{11} stress retards microcrack extension to a point where no crack growth is possible. The crack in Fig. 5(d) is longer than that physically possible for the grain orientations considered. Hence there is a *negative* stress raiser at the crack tip. From Fig. 5(c, d) it can be concluded that: (1) microcrack formation and growth does not relieve the tensile stresses within the grains ahead of the crack tip when grain boundary sliding is allowed; and (2) when no grain boundary sliding is permitted, the effect of a local stress concentrator is relieved by formation of a *short* microcrack. The length of the microcrack is dependent on the grain anisotropy.

These simulations are further proof (cf. [7]) that the elastic anisotropy mechanism acting alone is not strong enough to cause realistic microcracks in polycrystalline ice. Hence in all subsequent simulations, grain boundary sliding is allowed.

4.3. *Effect of grain anisotropy*

The effect of grain anisotropy on microcracking is studied by varying the orientation of the grain's orthotropic axis, ζ, with respect to a fixed global reference frame, and with respect to neighboring grains. The unit cell model described above allows arbitrary variation in orientation of all three grains making up the unit cell. For simplicity, and to reduce the number of variables, attention is focused on a symmetric distribution of grain orientations. In particular the following case is considered: $\zeta_A = 0$ and $\zeta_B = -\zeta_C = \zeta$. The influence of random grain orientations, ζ_A, ζ_B, ζ_C is considered elsewhere. Due to the symmetry of the boundary value problem, in all cases $J_y = 0$ and $J_x \neq 0$. Thus from equation (14) $\beta = 0$, $\mathscr{G} = J_x$ and the microcrack extends along the grain boundary.

In this section, the mean grain size of S2 is kept constant at $d = 5$ mm. The grain size is defined such that the area of the hexagonal grain is equal to the area of a circle with a diameter d.

†The grain size computed in [27] is based on a uniform sphere assumption and not on an equivalent area of a circle as in this paper. If the grain size used in the simulations, is computed in the same manner as in the experiment, the new stress range is: 1.55–1.9 MPa.

‡Provided the microcrack is longer than the "pop-in" length.

The variation of the energy released J_x, as the microcrack grows under constant uniaxial far field compression is plotted in Fig. 6(a). The whole range of grain orientations is considered: $0° \leqslant \zeta \leqslant 180°$. The microcrack length, l, is normalized by the facet length, a. The detail of Fig. 6(a) when the microcracks are short compared with the bubble radius, is plotted in Fig. 6(b). Figure 6(a, b) shows that there are regions of stable and unstable crack growth; a positive slope implies unstable crack growth while a negative slope corresponds to stable crack extension.

The defects located on the bubble surface release very little energy as they extend. This implies that they require a large far field compressive stress to nucleate. Once the nucleation stress is reached however, the defects grow unstably past the energy release peak into the stable regions, i.e. the region with a negative slope in Fig. 6(b). This is the "pop-in" length, also present in isotropic homogeneous materials [10]. The microcrack length increases with applied far field compression in a stable manner until the energy well is reached at approximately $l/a = 0.5$ [see Fig. 6(a)]. At this point the microcrack becomes unstable once again (the slope is positive), and grows to the neighboring triple point. Beyond this point, the direction in which the microcrack extends is dictated by the energy release criterion, equation (14), and is beyond the scope of this paper.

A different way to represent the stable and unstable crack growth is to plot the far field compressive stress required to propagate the microcrack, versus the normalized crack length, as done in Fig. 7. Equation (16) gives the nucleation stress corresponding to the released energy J_x. Figure 7 shows that a minimum of 1.4–1.7 MPa has to be applied for the microcrack to extend unstably to the full facet length. Reference [27] reports tests at $-10°$C on isotropic equiaxed granular ice with $d = 5$ mm† and reports the occurrence of the first microcrack at an uniaxial compressive stress range of 2.36–2.99 MPa. The stress range predicted is lower than observed experimentally due to the difference in the type of ice modeled and tested and due to the assumption of no shear stress transfer across grain boundaries. A more realistic assumption would be a visco-elastic response of the grain boundary.

Since the minimum stress occurs at approximately $l/a \approx 0.5$ and shorter cracks are stable‡, the origin of the defect is not critical. Here the original defect is assumed to be a surface flaw on the bubble, but can equally well be a decohered region on the grain boundary observed experimentally in [18].

Figures 6(a, b) and 7 show the effect of grain orientation on microcracking. In addition the variation of J_x with ζ is plotted in Fig. 8 for three different crack lengths. From these figures it is evident that grain anisotropy does not alter the nature of microcrack growth. The anisotropy does effect the length at which the microcrack becomes unstable, i.e. the position of the minimum in the energy J_x, and creates

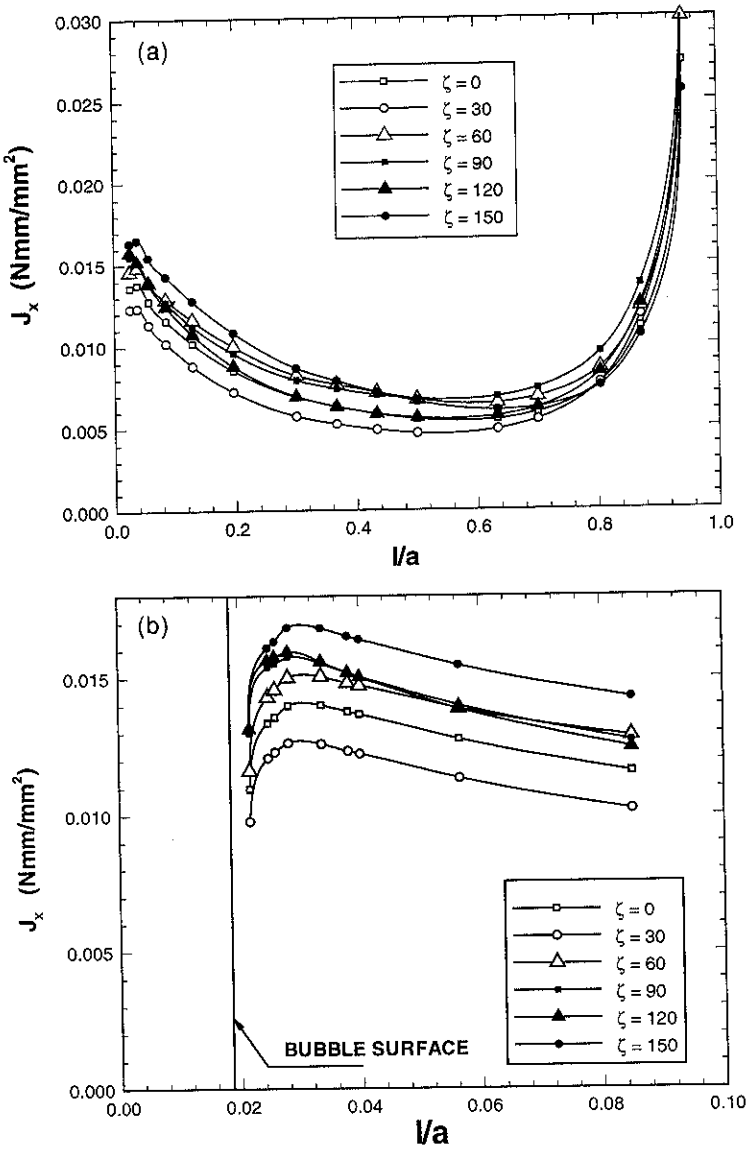

Fig. 6. (a) Variation of energy released, J_x, with normalized microcrack length for various grain orientations. (b) Variation of energy released, J_x, for short normalized microcrack lengths and for various grain orientations.

a band of stresses (or a band of J_x) which can cause microcrack growth. The maximum band width is 41% of the mean J_x and 21% of the mean stress required for microcrack growth. The mean values are taken at the point where the bands are maximum. It can be concluded that for a symmetric distribution of grain orientations within the unit cell, the anisotropy of the grains does not have a strong effect on the applied uniaxial compressive stress required to nucleate and propagate the microcrack.

4.4. *Effect of grain size*

The influence of grain size on the compressive stress required to nucleate and propagate a microcrack is studied in this section. The grain size, d, is varied in the range typically observed in polycrystalline S2 ice: $1\,\text{mm} \leqslant d \leqslant 10\,\text{mm}$. In addition, the effect of the grain orientation, ζ, is also considered. The bubble diameter, ϕ, is scaled linearly with grain size, from $\phi = 0.1$ mm for $d = 5$ mm.

The variation of the energy released, J_x, with microcrack length is plotted in Fig. 9 for three different grain sizes. The curve is drawn through the mean values of J_x; error bars indicate the width of the band produced by varying the grain orientations, ζ. From Fig. 9 it can be seen that the trends in J_x remain the same for different grain sizes. Although Fig. 9 shows that for fine grained samples, J_x varies very little with crack length, the applied compressive stress is inversely related to J_x [equation (16)]. Hence the variation in stress with microcrack length is not negligible, for all grain sizes. Also, as the grain

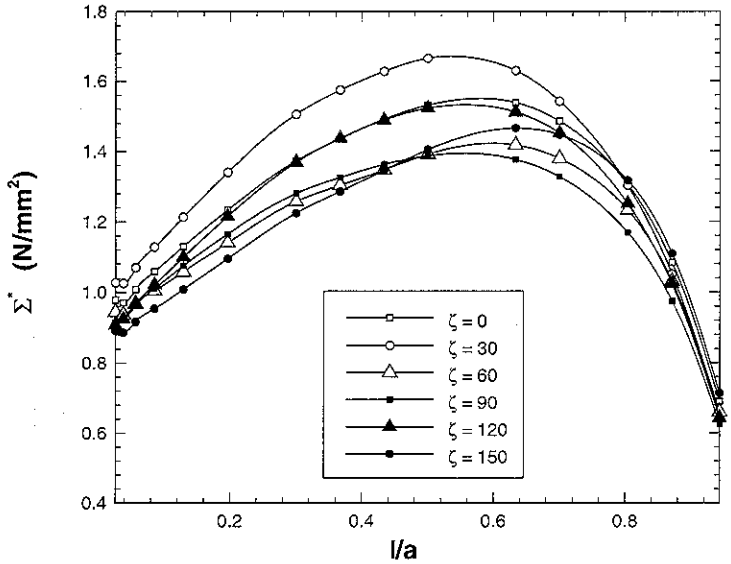

Fig. 7. Variation of applied compressive stress, Σ^* with normalized microcrack lengths for various grain orientations.

size decreases so the amount of energy released, J_x, also decreases. Thus, the compressive stress required to propagate the crack increases as the grain size decreases.

Figure 10 shows the stress required to lengthen the microcrack as a function of grain size for different crack lengths. The microcracking stress is proportional to $d^{-0.5}$.

The effect of grain anisotropy remains the same for polycrystalline ice of different grain sizes. The maximum band width is 41% of the mean J_x irrespective of d. Although this percentage is fixed, the magnitude of the variation in the far field stress is much larger for smaller grain sizes where the microcracking stress is large (see Fig. 10). Hence the grain anisotropy should produce more measurable scatter in microcracking stress as the polycrystal becomes fine grained.

The above discussion suggests that in real polycrystal samples, loaded at sufficiently fast rates to ensure linear stress–strain response, there should exist two populations of microcracks. The first group of microcracks have lengths in the range $0.1 \leqslant l/a \leqslant 0.5$. The second group have lengths equal to, or longer than the grain facet lengths. References [11, 28] report

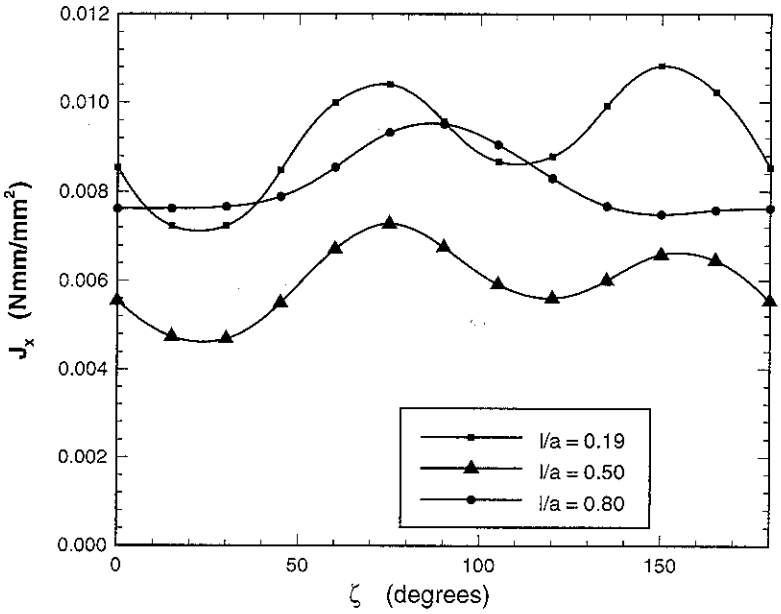

Fig. 8. Variation of energy released, J_x, with grain orientation, ζ, for various normalized microcrack lengths.

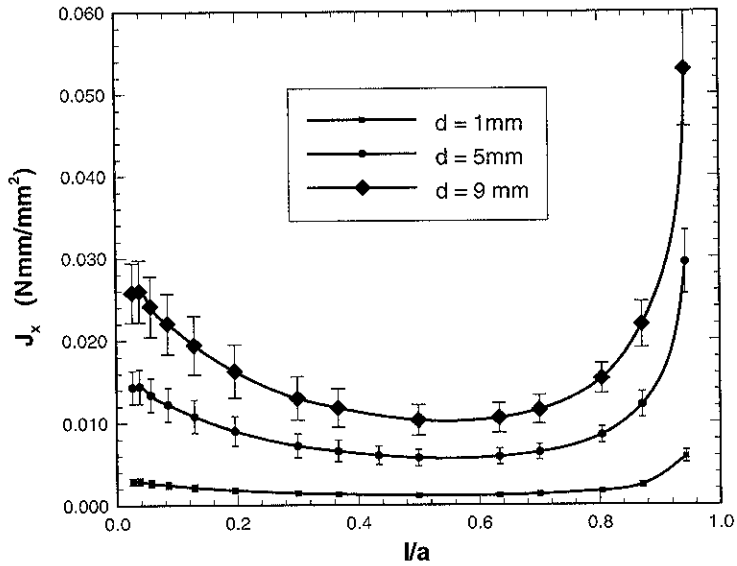

Fig. 9. Variation of energy released, J_x, with normalized microcrack length, l/a, for various grain sizes.

experimental evidence of stable microcrack extension until a critical length is reached, at which point the microcrack growth becomes unstable. Although a normalized microcrack length is reported, the normalizing length is not the facet length. Further, due to the relative coarseness of the grains compared to the specimen size, no conclusion can be reached as to the fraction of the facet length at which the microcracks became unstable.

5. CONCLUSION

This paper examines the grain boundary sliding mechanism, as a possible cause of microcracking at moderately high rate of quasi-static uniaxial compression where the response of the polycrystal is almost linear. Results show that without allowing relative motion of the grains along the grain boundary, unrealistically high stresses are required to nucleate and propagate a microcrack; in addition the resulting microcracks are much shorter than those observed experimentally. By assuming, for simplicity, free boundary sliding, the stresses required to nucleate and propagate a grain boundary microcrack, become more realistic. Due to the assumption of free slip, the stresses are under predicted.

Simulations with a unit cell model which allows variation of grain orientation and grain size, show that at first a large stress is required to nucleate a flaw located at the triple point. The flaw "pops-in" and

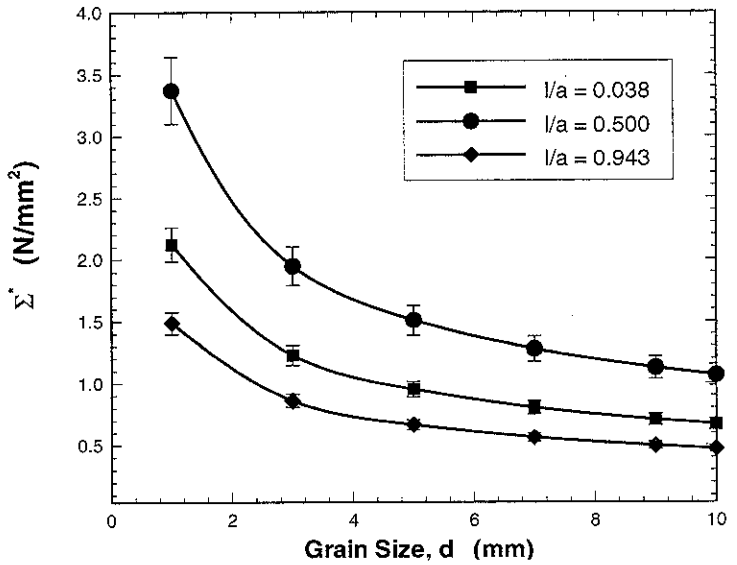

Fig. 10. Far field compressive stress, Σ^* required to extend a microcrack of varying length versus grain size, d.

then increases in length with increasing applied compression. When the microcrack extends to approximately half the facet length it grows unstably to the neighboring triple point. The effect of grain anisotropy is to shift this point of instability and to produce a band of stresses required to increase the microcrack length. The maximum band width is approx. 21% of the mean stress.

Varying the grain size does not change the microcrack behavior; the microcrack extends stably after the "pop-in" length and then becomes unstable. The stress required to extend the microcrack a fixed fraction of the facet length is inversely proportional to the square root of the grain size. The analysis implies that two populations of microcrack lengths should exist: (i) microcracks which are shorter than about half the facet length; and (ii) microcracks which extend at least over the entire facet length.

The effect of random variation of grain orientations, and the effect of confining the specimen as well as visco-elastic modeling of the grain boundary region warrant further investigation.

Acknowledgements—The authors thank Professor Vijay Gupta of Dartmouth College for providing them with his manuscripts only recently submitted for publication. This research was supported by the Office of Naval Research (Grant No. N00014-92-J-1208) and by the Minerals Management Service (Contract No. 14-35-0001-30735).

REFERENCES

1. L. W. Gold, *Phil. Mag. A* **26,** 311 (1972).
2. E. M. Schulson, *Cold Reg. Sci. Tech.* **1,** 87 (1979).
3. D. M. Cole, *Cold Reg. Sci. Tech.* **15,** 79 (1988).
4. N. K. Sinha, *Proc. IUTAM Conf., Deformation and Failure of Granular Materials*, pp. 323–330 (1982).
5. N. K. Sinha, *J. Mater. Sci.* **19,** 359 (1984).
6. S. Shyam Sunder and M. S. Wu, *Cold Reg. Sci. Tech.* **18,** 29 (1990).
7. V. Gupta, R. C. Picu and H. J. Frost, *Ice Mechanics, ASME, AMD* **163,** 199 (1993).
8. A. E. Carte, *Proc. Phys. Soc.* **77,** 757 (1961).
9. J. H. Currier and E. M. Schulson, *Acta metall.* **30,** 1511 (1982).
10. C. G. Sammis and M. F. Ashby, *Acta metall.* **34,** 511 (1986).
11. N. P. Cannon, E. M. Schulson, T. R. Smith and H. J. Frost, *Acta metall. mater.* **38,** 1955 (1990).
12. V. Tvergaard and J. W. Hutchinson, *J. Am. Ceram. Soc.* **71,** 157 (1988).
13. P. V. Hobbs, *Ice Physics.* Clarendon Press, Oxford (1974).
14. A. K. Chatterjee and H. H. G. Jellinek, *J. Glaciol.* **10,** 293 (1971).
15. P. Barnes, D. Tabor and J. C. F. Walker, *Proc. R. Soc. Lond. A* **324,** 127 (1971).
16. J. Tatibouet, J. Perez and R. Vassoille, *J. Physique* **48,** C1-197 (1987).
17. L. W. Gold and A. Traetteberg, *Proc. 2nd Symp. on Application of Solid Mechanics*, Dep. Mech. Eng., McMaster Univ., Hamilton, pp. 1–15 (1974).
18. R. C. Picu and V. Gupta, Observation of Crack Nucleation in Columnar Ice Due to Grain Boundary Sliding. Submitted.
19. M. A. Hussain, S. L. Pu and J. Underwood, *Fracture Analysis, ASTM STP 560*, pp. 2–28. American Society for Testing and Materials (1974).
20. V. Z. Parton and E. M. Morozov, *Mechanics of Elastic-Plastic Fracture*, 2nd edn. Hemisphere, Washington (1989).
21. B. Budiansky and J. R. Rice, *J. appl. Mech.* **40,** 201 (1973).
22. J. R. Rice, *J. appl. Mech.* **35,** 379 (1968).
23. P. H. Gammon, H. Kiefte, M. J. Clouter and W. W. Denner, *J. Glaciol* **29,** 433 (1983).
24. W. M. Ketcham and P. V. Hobbs, *Phil. Mag. A* **19,** 1161 (1969).
25. V. R. Parameswaran and S. J. Jones, *J. Glaciol.* **14,** 305 (1975).
26. C. Zener, *Phys. Rev.* **60,** 906 (1941).
27. P. Kalifa, P. Duval and M. Ricard, *8th Int. Conf. Offshore Mech. and Arctic Engineering*, The Hague, pp. 19–23 (1989).
28. E. M. Schulson, G. A. Kuehn, D. E. Jones and D. A. Fifolt, *Acta metall. mater.* **39,** 2651 (1991).